On the Effects of a Midocean Ridge on the General Circulation: Numerical Simulations with an Eddy-Resolved Ocean Model

JACQUES VERRON AND CHRISTIAN LE PROVOST

Institut de Mécanique de Grenoble, 38402 St. Martin d'Hères Cédex, France

WILLIAM R. HOLLAND

National Center for Atmospheric Research, Boulder, CO 80307

(Manuscript received 9 February 1986, in final form 4 September 1986)

ABSTRACT

High resolution ocean general circulation model experiments were carried out to investigate the effects of a midocean ridge on the eddy field and the mean circulation on the basin scale. A quasigeostrophic two-layer model was used. Long term statistics were computed for a detailed comparison with the flat bottom case. An eddy-driven anticyclonic gyre, locked over the topography, appears as a new feature of the deep circulation pattern. The eddy energy radiation in both layers is strongly constrained by the topography. Insofar as surface currents are concerned, the ridge acts, to a limited extent, as a new western boundary for the eastern basin.

1. Introduction

Ridges are the major feature of ocean bathymetry. They are present in most of the ocean basins and their influence on general oceanic circulation has been a matter of speculation for a long time. For example, it has been noted that ridges can cut off a global deep water mass in one basin from a neighbouring mass in another. The Mid-Atlantic Ridge is one of the most remarkable ridge systems in the world oceans. Many observations have shown correlations between certain dynamical anomalies and the presence of this large scale topographical feature (MODE, POLYMODE, TOPOGULF).

In the North Atlantic, the ridge is located in portions of the general circulation where the surface intensified mean flow is relatively weak and the currents are dominated by eddy dynamics. The role of bottom topography has not yet been studied, especially at large scales, with eddy resolving general circulation models (EGCM). However, the EGCM's have recently shown their ability to simulate realistically the distribution of the variability in an ocean basin, for example in reproducing the multiple sources of eddy energy in the North Atlantic basin. The development stage of eddy-resolved models is far from complete. In particular, future studies will require the inclusion of more realistic forcing, coupled with a satisfactory representation of the bottom topography. The aim of the present study is to contribute towards meeting these requirements.

Two numerical experiments were performed using an eddy-resolving model. The second experiment differs from the first by the introduction of a ridge-type topographic feature. The model we are using belongs to the category of eddy-resolving gyre-scale models that have already been studied by Holland and Lin (1975a,b), Robinson et al. (1977), Semtner and Mintz (1977), and Holland (1978). The analysis of the major processes occurring in these simulations by Haidvogel and Holland (1978), Harrison and Robinson (1978, 1979), Semtner and Holland (1978), Harrison and Holland (1981), Rhines and Holland (1979), and Holland and Rhines (1980) have provided us with an understandable picture of the main characteristics of the general oceanic circulation and their statistical properties. Most of these features are reproduced in the first basic flat bottom experiment carried out in the context of this study.

The large scale circulation, induced by an antisymmetric wind stress curl acting on the upper layer, is dominated by an intense jet penetrating eastward in the middle of the basin, at the latitude of the zero wind-stress curl. The amplitude of this highly nonlinear mean flow in the upper layer is limited by barotropic and baroclinic instabilities and the mesoscale eddies, spontaneously generated, affect the statistical equilibrium of the global circulation in a fundamental way. In this upper layer, by transporting relative vorticity across the zero wind stress curl latitude, they contribute to the global vorticity balance between the two half basins. Eddies induce strong westward recirculation patterns which occur beside the jet, leading to intense "inner" gyres, embedded in the Sverdrup-like "outer" gyres which occupy the rest of the basin. The mesoscale eddy field is also responsible for downward propagation of energy, thereby inducing eddy activity in the lower layer

and leading to abyssal, time mean gyres that contribute significantly to total mass transport in the ocean. As was noted by Schmitz and Holland (1982), the inner-gyre upper layer system and its lower layer equivalent are roughly consistent with Worthington's (1976) picture of the Gulf Stream system, and the outer southern basin gyre with the global subtropical North Atlantic circulation.

The aim of the present work is to examine to what extent the presence of a large scale topographic feature like the Mid-Atlantic Ridge might alter the preceding picture by changing the stability characteristics of the flow, by causing different vertical distributions of eddy energy and by hindering the horizontal propagation of eddy energy. First, we briefly summarize the main features of the quasigeostrophic two-layer model and describe the design of the numerical experiments performed. In the second part, we present a diagnostic analysis of the differences that appear in the mean and eddy fields, owing to the topography. Finally, we summarize the overall effects of the ridge and tentatively interpret the underlying causes of these results.

2. The numerical experiments

a. Main features of the model

The model we are using is a two-layer quasigeostrophic model. It is an eddy-resolving general circulation model in the sense that the geometry is basin-size and that the horizontal resolution is fine (20 km). Because of the resolution (and small dissipation) it has the ability to develop strong instabilities and to give a picture of an ocean which is fully turbulent. Thus, extended calculations are performed in time to reach a "statistically steady state" in which eddies and mean flow are in mutual balance.

Details of the model formulation, the geometry, and the nondimensional parameters that govern the flow are given elsewhere. Basically, the model is the one presented by Holland (1978). Let us simply note here that it is a two-gyre, wind-driven case with a steady sinusoidal wind stress (1 dyn cm^{-2}) in a square $L \times L$ basin (4000 km on a side). Bottom friction ($\epsilon = 10^{-7}$ s^{-1}) and a high order biharmonic lateral friction ($A_4 = 8 \times 10^9$ m^4 s^{-1}) provide the dissipative mechanisms. The layer depths are $H_1 = 1000$ and $H_3 = 4000$ m. The Coriolis parameter is

$$f = f_0 + \beta_0\left(y - \frac{L}{2}\right)$$

where

$$f_0 = 9.3 \times 10^{-5}\ \text{s}^{-1}$$

(corresponding to latitude 40°) and

$$\beta_0 = 2 \times 10^{-11}\ \text{m}^{-1}\ \text{s}^{-1}.$$

The reduced gravity is $g' = 0.02$ m s^{-2} which corresponds to an internal Rossby radius of 43 km.

The two-layer vertical structure is very crude. Flierl (1978) has studied the calibration of the two-layer system for a variety of flows. He has shown that the best-fit parameters vary widely depending on the phenomenon under investigation. In particular a study of topographic effects requires an optimal choice of mean depths for the upper and lower layers quite different from the optimal choice required for a study of nonlinear effects. In the present numerical experiments, with many competing processes, we have chosen the same parameters as in the basic flat-bottom experiment examined by Holland (1978) and Schmitz and Holland (1982). The model has not been optimized for the study of any set of isolated processes and it should be kept in mind that we can achieve here at best a qualitative description of the various effects.

The equations of the model are

$$\frac{\partial}{\partial t}(\Delta\psi_1) + J(\psi_1, \Delta\psi_1 + f_1) + \left(\frac{f_0}{H_1}\right)w_2 = \left(\frac{1}{H_1}\right)\text{curl}_z\tau - A_4\nabla^6\psi_1$$

$$\frac{\partial}{\partial t}(\Delta\psi_3) + J(\psi_3, \Delta\psi_3 + f_3) - \left(\frac{f_0}{H_3}\right)w_2 = -\epsilon\Delta\psi_3 - A_4\nabla^6\psi_3$$

$$\frac{\partial}{\partial t}(h_2) + J(\psi_2, h_2) = w_2$$

where

$$h_2 = \left(\frac{f_0}{g'}\right)(\psi_3 - \psi_1)$$

$$\psi_2 = \left(\frac{H_3\psi_1 + H_1\psi_3}{H_1 + H_3}\right)$$

$$f_1 = f$$

$$f_3 = f + f_0\left(\frac{h_0}{H_3}\right)$$

and $h_0(x, y)$ is the height of the topography. Other notations are standard. These equations can also be expressed as statements about the conservation of the potential vorticity:

$$\frac{DQ_1}{Dt} = \left(\frac{1}{H_1}\right)\text{curl}_z\tau - A_4\nabla^6\psi_1$$

$$\frac{DQ_3}{Dt} = -\epsilon\Delta\psi_3 - A_4\nabla^6\psi_3$$

where

$$\frac{DQ_i}{Dt} = \frac{\partial Q_i}{\partial t} + J(\psi_i, Q_i)$$

$$Q_1 = \Delta\psi_1 + f + f_0\left(\frac{h_2}{H_1}\right)$$

$$Q_3 = \Delta\psi_3 + f + f_0\left(\frac{h_0}{H_3}\right) - f_0\left(\frac{h_2}{H_3}\right).$$

b. Design of the experiments

The main objective of this study is to identify the possible influences of a midocean ridge on the wind- and eddy-driven circulations. The chosen strategy is to run two experiments in parallel, experiment 1 incorporating a flat bottom and experiment 2 a ridge.

The quasigeostrophic (QG) formulation and the two-layer vertical resolution have decided advantages. We expect to produce flow dynamics which are simple compared to the real ocean. In this way, major topographic effects can be made more comprehensible. Also it is possible for a reasonable computing cost to run several years of simulation and thus to obtain a quasi-stationary state in which the necessary eddy-statistics can be computed.

There are, of course, drawbacks to this choice. First, the inclusion of topography in the QG context is straightforward only if the amplitude of the bathymetric variation is small compared to the mean depth of the lower layer. This corresponds to the QG assumption that variations in layer thicknesses are small compared to the mean layer thicknesses. The dynamical effect of the bathymetric height could thus be considerably distorted. Consequently, the height of the ridge introduced here has been reduced considerably compared for example to the Mid-Atlantic Ridge. Second, we know from Schmitz and Holland that some QG simulations are consistent with several properties of the data base in the North Atlantic and a variety of observed characteristics are approximately reproduced. But this is true only as long as the comparison is undertaken at analogous positions relative to the distribution of eddy and mean fields. This is because a discrepancy occurs in the model in attempting to simulate the zonal scale of penetration for the Gulf Stream and its associated eddy field. This inadequate zonal penetration (by a factor of 2 or so) is liable to result from an incorrect control of the subtle balance between the jet stream extension and the intensity of its instability (Holland and Schmitz, 1985). By reducing the latter, a better penetration of the jet can be obtained, but then simultaneous agreement with observations of the mean flows and their associated eddy fields in the upper and lower layers is difficult to achieve. This problem is also associated with the lack of vertical resolution and the calibration of the layers as mentioned earlier. Consequently, it was not possible to incorporate the ridge in the basin in strict agreement with the geographical position of the Mid-Atlantic Ridge. Its position was chosen instead in such a way that the ridge lies in a region of significant and realistic eddy activity.

The schematic model ridge is a meridionally oriented barrier. The zonal sections have a Gaussian shape. At the north and south ends, the height is smoothed down to zero, in order to obtain (f/H) contours following exactly the north and south boundaries of the basin and to thus avoid vorticity inputs at these two boundaries. The topographic height is written as:

$$h_0(x,y) = \left(\frac{h_{\max}}{2}\right) e^{-[(x-x_r)/a]^2}\left[\tanh\left(\frac{y-y_a}{d}\right) - \tanh\left(\frac{y-y_b}{d}\right)\right]$$

where x_r is the location of the ridge axis (1000 km from the western boundary), a is the characteristic width (300 km), $h_{\max}$ is the maximum height (500 m), y_a and y_b are the southern and northern latitudinal limits of the ridge, and d is the characteristic decaying length scale for the preceding limits (Fig. 1). These choices result in a large scale slope of around 1.6×10^{-3}, that is an equivalent β-effect of 4×10^{-11} m^{-1} s^{-1}. Thus, the ridge will be as important as β in Rossby wave dispersion. Note that the jet penetration in the flat bottom experiment is about 750 km, thus bringing mean and eddy flows to the vicinity of the ridge in the second experiment.

c. Statistical considerations

For the purpose of examining the final statistically steady state of the model, time mean and eddy quantities are considered. As was shown by Holland and Rhines (1980), perfect equilibrium in the flat-bottom experiment will give time-averaged quantities that should be perfectly symmetric (or antisymmetric) about midlatitude of the basin. However, even 3600 day averages still show some degree of asymmetry. But from a detailed study of the statistical stability of the various quantities over periods varying from about 100 to 3600 days, Holland and Rhines suggested that an averaging time of 1800 days provides an accurate representation of the main quantities of the fields. The discrepancy is not greater than 10%–15%, even if perfect stability is still not completely achieved. The statistics for the topographic experiment carried out here are assumed to be the same. Thus to conserve computing time, the length of the analysed time series was chosen as 1800 days in both experiments. Consequently, the sequence of calculations was as follows: first, a spinup phase of 3600 days without topography is run. Then for the flat bottom case a further 1800 day run is made from which the statistics of experiment 1 are computed. Experiment 2 is also started from the initial 3600 day flat bottom run. After the topography is introduced, a further 600-day adjustment period is allowed and then a further 1800 day run is conducted from which the statistics of experiment 2 are calculated.

3. Results of the comparative experiments

a. The mean fields

1) THE UPPER LAYER

The numerical experiments yielded time-averaged streamlines and temperature (or interface height) fields as shown in Fig. 2. These give Eulerian mean velocity patterns which might be schematically described in the

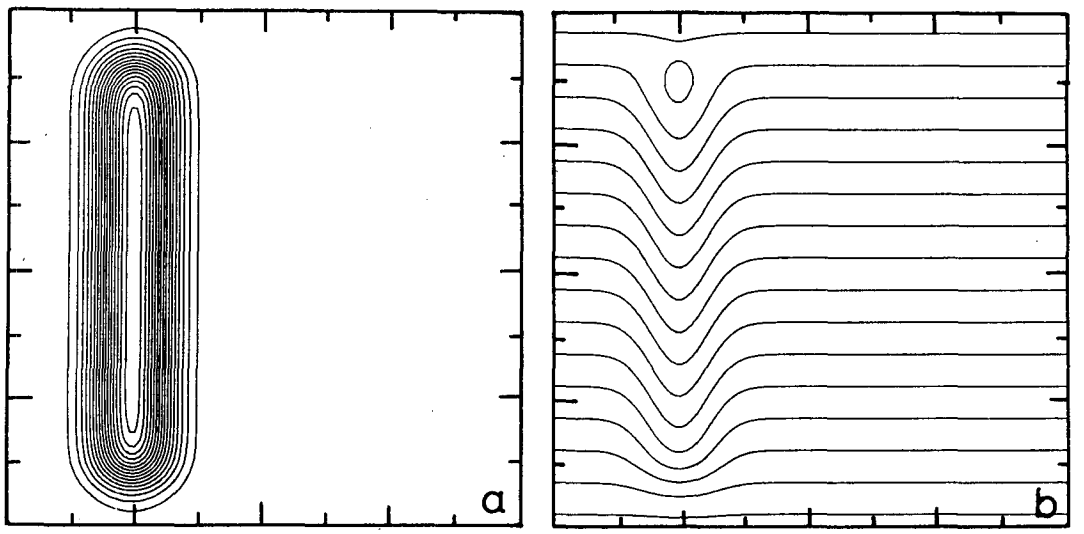

FIG. 1. The schematic ridge (a) and the associated f/H contours (b).

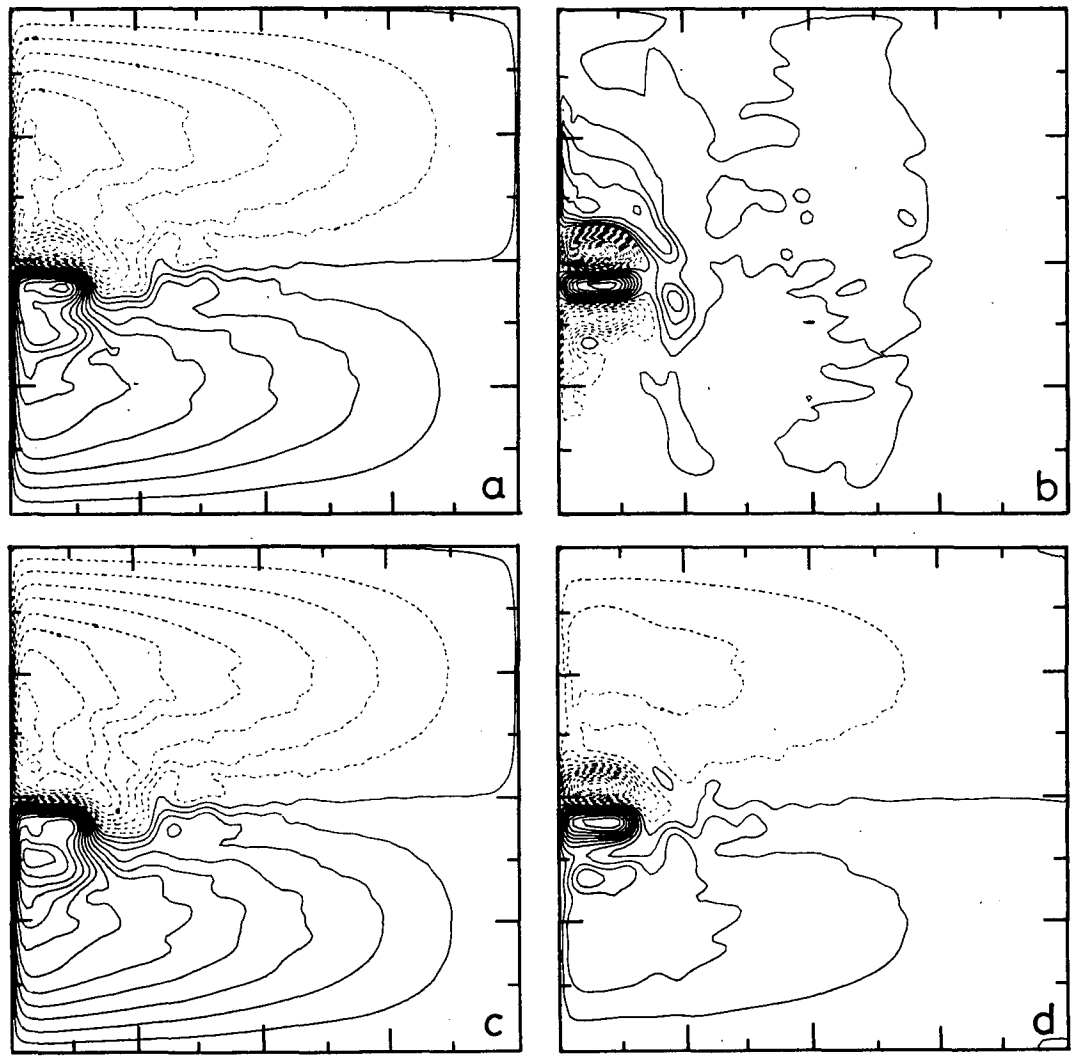

FIG. 2. The mean field for experiment 2 (a) ψ_1 (CI = 5000 m^2 s^{-1}), (b) ψ_3 (CI = 1250 m^2 s^{-1}), (c) h_2 (CI = 20 m), and (d) barotropic mode ψ (CI = 2000 m^2 s^{-1}). Dashed lines are for negative values except for h_2.

upper ocean, as a pair of inertial gyres with broad and weak Sverdrup circulations filling out the rest of the basin. In the flat bottom case, a free jet (a simulated Gulf Stream) divides the gyres, drawing off boundary current fluid equally from north and south. In the topographic case the jet is deflected southwards as it reaches the ridge (Fig. 2a). The mean velocity profile as given by meridional sections is not strongly affected. The eastward penetration of the jet is reduced, from around 750 to 600 km. But the jet length determined by following its mean axis stays about the same. The relevance of the apparent southward shifting (also observable in the deep layer) of the latitude at which the jet separates from the coast is not clear; this may be due to the inherent inaccuracy of the averaging process.

East of the ridge some recirculating slow flows are observed in two quasi-symmetric regions, the total area of which is around 600 km × 600 km. They are embedded in the Sverdrup circulation that still dominates the global circulation in that part of the basin. But the local dynamics are those of a short, and relatively slow (10 cm s^{-1}), inertial jet associated with its two recirculating small gyres (Fig. 3). This subregion is also distinguishable in the mean potential vorticity pattern for the upper layer, because of the local homogenization of Q (Fig. 9).

2) THE LOWER LAYER

The deep mean Eulerian circulation is driven entirely by eddies. In the real ocean there is a superposition of thermohaline circulation and eddy-driven circulation. Only the latter is present in our simulation where no thermohaline forcing occurs. Moreover, a purely steady model flow will not exhibit any topographic signature since there are no interfacial stresses between the two layers.

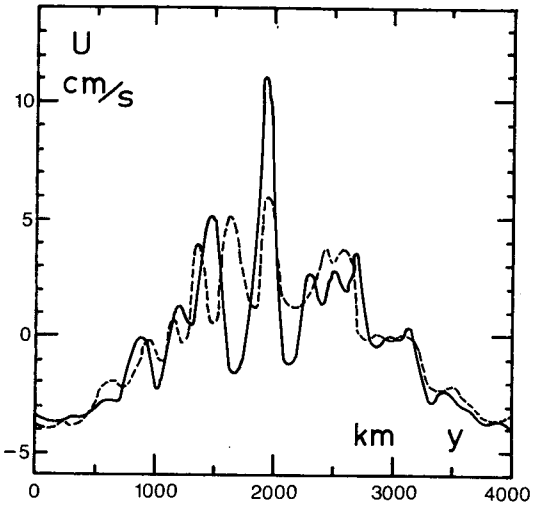

FIG. 3. Mean velocity section at x = 1400 km in the upper layer for experiment 1 (dashed line) and 2 (solid line).

The eastward mean jet, which is generated in the deep water under the surface jet, is not strongly affected by the presence of the topography. It shortens from about 750 to 700 km but it does not undergo any significant latitudinal shifting. However, the recirculating flow is intensified and the corresponding jet has a sharp profile when returning westward at a velocity of around 10 cm s^{-1}.

The general circulation in the deep layer is modified by the appearance of a new anticyclonic deep gyre over the ridge which is connected to the outer northern gyre (Fig. 2b). There is a general reinforcement of the cyclonic cells in the deep ocean which offsets the vorticity input due to the topography. Another general feature is that the ridge acts to confine the more intense deep circulations to the western part of the basin.

b. The eddy fields

1) EDDY KINETIC ENERGY DISTRIBUTION IN THE UPPER LAYER

In Fig. 4a KE'_1 maps are presented for the flat bottom case and in Fig. 4b for the topographic case. For experiment 1, the situation is completely symmetric. This is particularly so for the KE'_1 distribution; the energy is concentrated in the region of instability of the free jet, with a maximum along its axis. The energy levels fall off rapidly and symmetrically to the south, the north and the east by two orders of magnitude within 100 km. It should be noted that the energy levels (up to 2000 cm^2 s^{-2} in the core of the jet) are close to the recent observations in the Gulf Stream (Richardson, 1983). Far from the active jet stream region, the energy levels are distributed as circles centered on the extremity of the jet, and decreasing down to a few cm^2 s^{-2}.

The KE'_1 distribution for the topographic case differs from the preceding one in four main ways:

(i) the maximum energy levels, still centered along the axis of the jet, are shifted southward;

(ii) a tongue of intermediate level eddy energy (between 10 and 100 cm^2 s^{-2}) appears on the eastern flank of the ridge, along the axis of the jet;

(iii) on the western side of the ridge the KE'_1 levels do not decrease symmetrically from the axis of the jet; the southern part is more energetic in the intermediate level range;

(iv) in the open ocean the fluctuating energy distribution is no longer circularly distributed, but zonally polarized. In the narrow central part of the basin the kinetic energy is slightly enhanced while it decreases in the northern and southern parts.

2) EDDY KINETIC ENERGY DISTRIBUTION IN THE LOWER LAYER

In the deep ocean the spatial distribution of KE'_3 (Fig. 5) has some similarity with the upper layer but, as one might expect, the kinetic energy levels are much

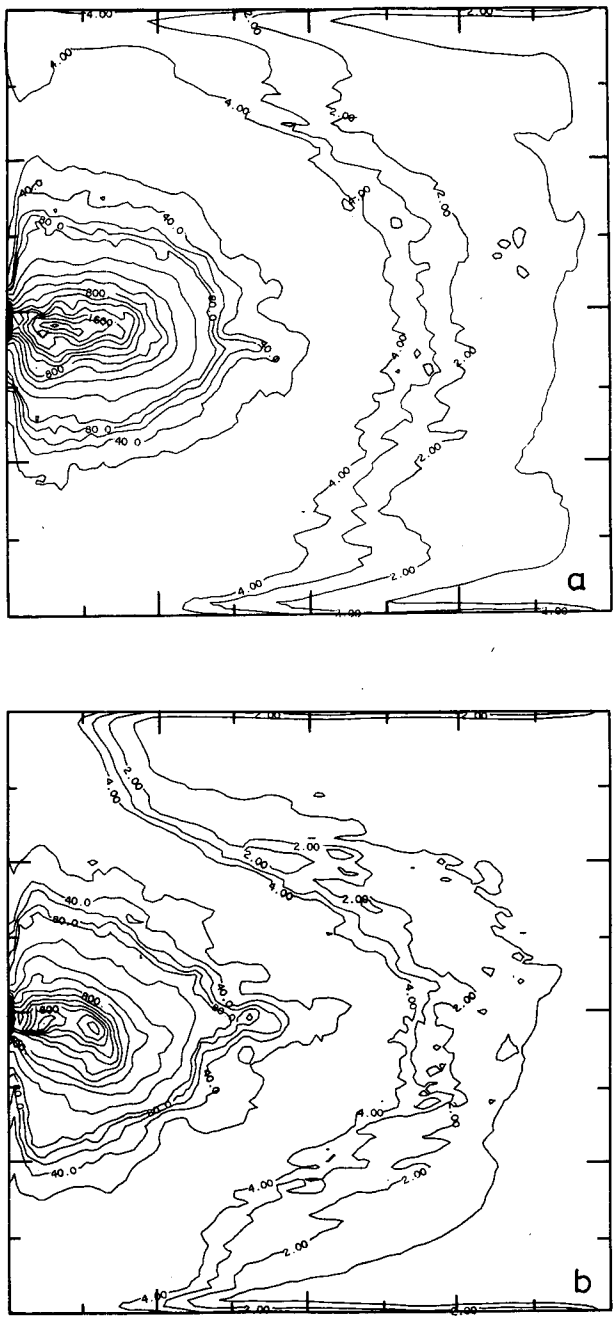

FIG. 4. Maps of eddy kinetic energy (KE'_1) in the upper layer from (a) experiment 1 and (b) experiment 2.

lower. Beneath the core of the jet, the maximum values are reduced by a factor of 10 (180 $cm^2 s^{-2}$ for experiment 1). In the far field, however, this ratio is only 2; the response of the ocean in that area is mainly barotropic through Rossby waves. In spite of this decrease, the important point is the increase in the relative eddy/mean activity in the deep layer.

In the presence of the ridge, the KE'_3 distribution (Fig. 5b) is much more strongly modified than was the case for the upper layer.

(i) the area of maximum levels is now larger, with an important spreading out on the southern side of the jet, along the foot of the ridge, but the highest values are a little lower (160 $cm^2 s^{-2}$).

(ii) in the western area, limited by the ridge, the eddy activity is more intense in a general way. In particular, all the southern sub-basin is filled with intermediate level kinetic energy (between 10 and 100 $cm^2 s^{-2}$). Moreover, there is a strong assymmetry for that distribution and two regions are favored: the southwest

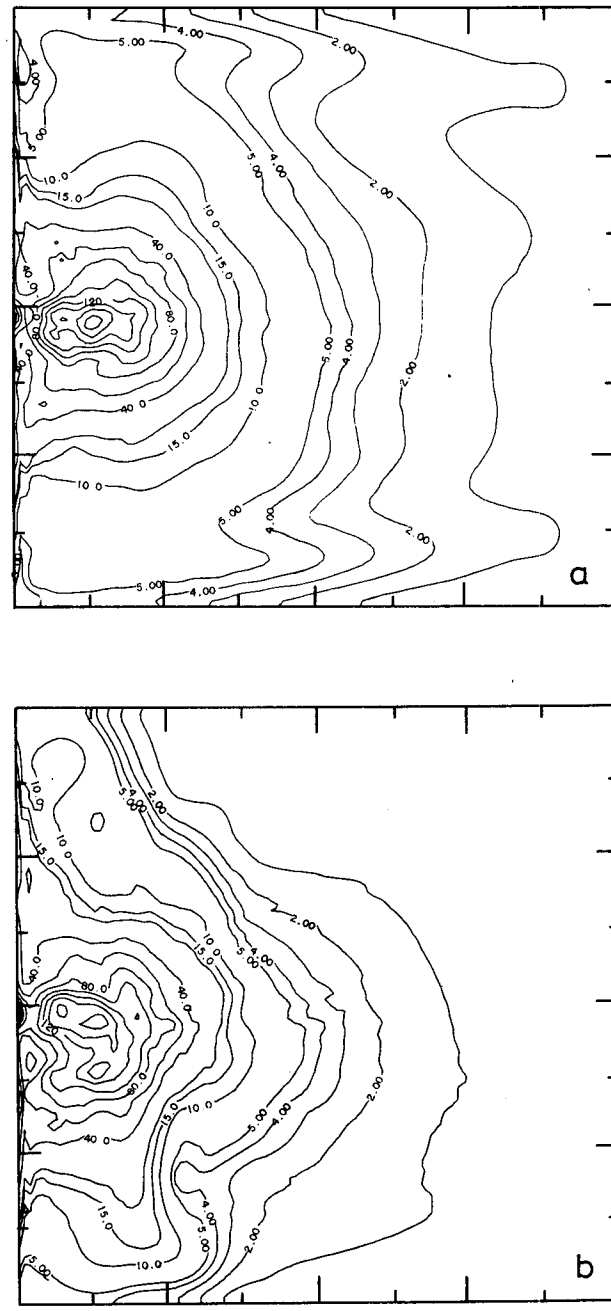

FIG. 5. Maps of eddy kinetic energy (KE'_3) in the lower layer from (a) experiment 1 and (b) experiment 2.

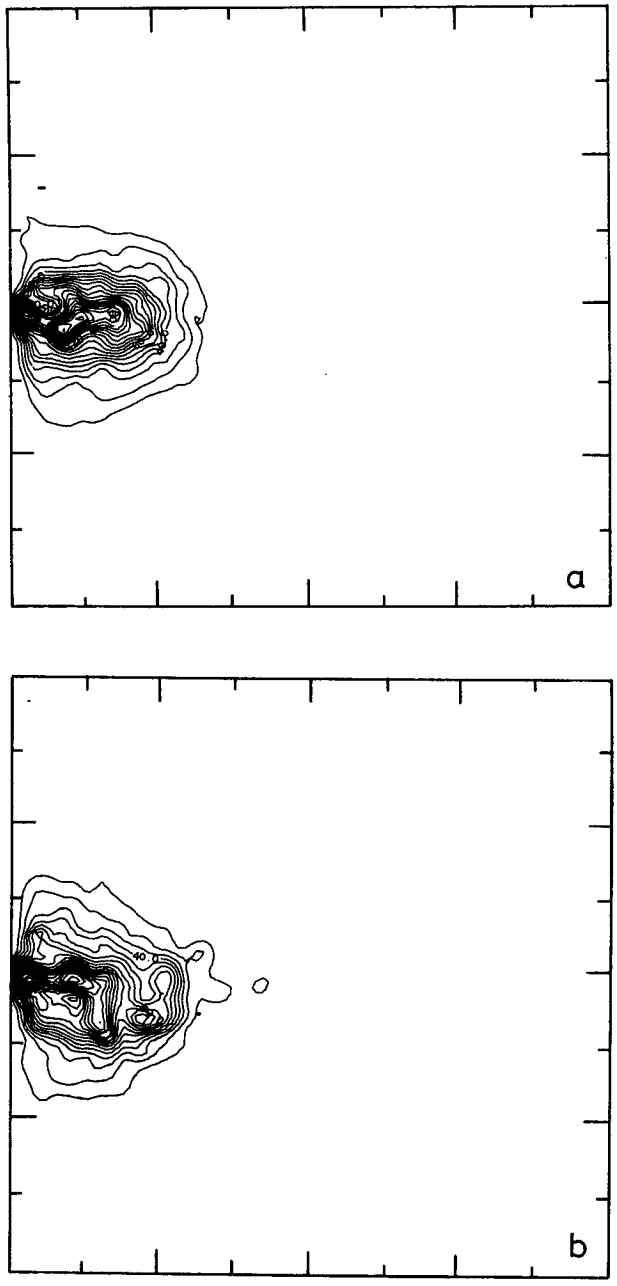

FIG. 6. Maps of eddy potential energy (PE′) from (a) experiment 1 and (b) experiment 2. (CI = 10 cm^2 s^{-2}).

flank of the ridge and the northwest boundary of the domain.

(iii) on the eastern side of the ridge the eddy energy (low level) is reduced by a factor of 2. However, the same zonal polarization, already observed in the upper level, can be observed along the midlatitude of the basin.

(iv) the tongue of higher eddy energy along the axis of the jet on the eastern flank of the ridge, which occurred in the upper layer, was not observed.

3) EDDY POTENTIAL ENERGY DISTRIBUTION

The PE′ maps are similar to the KE′ maps with a maximum along the axis of the jet. The essential point to be noticed here is the striking pattern of this field in experiment 2, in the area of maximum variability (Fig. 6). Two tongues with higher energy levels can be seen here, along the jet, one running southwards at the western foot of the ridge, the other extending northwards just east of the ridge crest. This is a signature of the meandering activity of the upper layer jet over the ridge. This activity is characterized by a smaller scale variability, local meanders with periods of about 30 days compared to a range of 50 to 100 days for regular meanders in the jet. Induced variability of the local thermocline is likely to explain the augmented eddy potential energy in that area. Dantzler (1977) mapped out the eddy potential energy in the North Atlantic and found a suggestion of such higher magnitude values along the eastern slope of the Mid-Atlantic Ridge in midlatitudes.

c. Transports

A generalized streamline pattern is outlined schematically in Fig. 7. Schmitz and Holland (1982) have

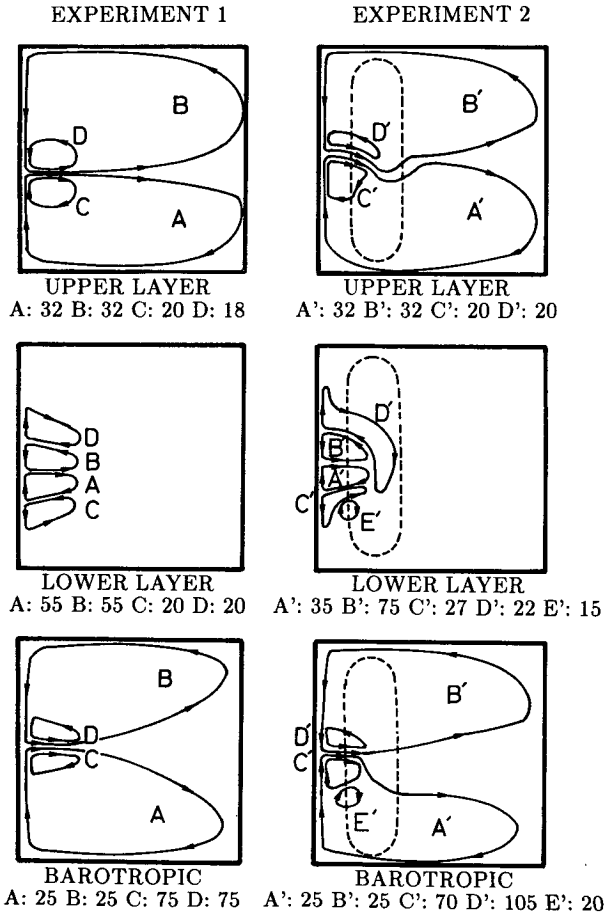

FIG. 7. Schematic streamline patterns and transports for the upper layer, lower layer and total-depth mean flows.

identified two scales of time averaged circulation and two types of gyres. Each half-basin in the upper layer has a large-scale outer gyre (A and B), basically a Sverdrup circulation, and a smaller-scale inner gyre (C and D), which are the jet recirculations. Each half-basin in the lower layer has two gyres at the size of the smaller scale: one is near the jet (A and B) and could correspond to the surface recirculating flows; the other is an outer pair of gyres (C and D).

As mentioned earlier, this mean flow pattern may be roughly consistent with some classical pictures of the North Atlantic circulation. The existence of the deep abyssal gyres, which appear as new elements in these pictures, is discussed in detail by Holland and Rhines (1980). The topography alters in several aspects this global scheme; some new features and weak gyres are present.

Figure 7 also indicates the mass transport in the different gyres. In the upper layer it should be noted that the transport (defined as the flow going through the outer half of gyres A and B) corresponds approximately to a Sverdrup transport $2\pi\tau_{max}/\rho\beta_0 = 31.4$ Sv (1 Sv $\equiv 10^6$ m^3 s^{-1}). The presence of the inner gyres C and D increases this transport to a total value of 52 Sv, for each gyre. The presence of the topography does not modify these results.

This is not the case for the lower layer. In the flat bottom case the flow patterns, which are quite symmetrical, transport 55 Sv in A and B gyres and 20 Sv in C and D. The presence of the ridge introduces an asymmetry between these gyres: the cyclonic ones on the north are more intense (up to 75 Sv for B′ and 27 Sv for C′) and the main anticyclonic recirculating gyre (A′) on the south is reduced to 35 Sv.

These features show clearly in the barotropic mode (the total vertically averaged transport). Although the large scale subtropical gyre and its northern counterpart transport the same 25 Sv (with and without topography), the inner Gulf Stream system is completely different in the two experiments. In experiment 2 the total transport in the northern gyre reaches 130 Sv because of the enhancement of the inner gyre D′; in the southern gyre the maximum is only 95 Sv, but a secondary gyre (E′) transporting approximately 20 Sv appears on the south of the inner gyre C′.

The topography of the interface is also significantly modified by the presence of the ridge; the upward deviation of the interface on the northern side of the jet is reduced from 200 to 180 m, while the downward deviation in the southern gyre is increased to 240 m. The appearance of pools of constant temperature waters must also be pointed out on each side of the jet, on the eastern flank of the ridge, corresponding to the recirculating inertial-flow regions previously mentioned.

d. Energy analysis

A comprehensive understanding of these complex turbulent numerical experiments can be developed only through extensive analysis of the results. Global energy analysis is one way of going about this. When the flow is examined over a period of time in the final statistically steady state, the time dependent variables can be split up into a time-mean part and a fluctuating part. In particular, this can be used to compute the energy transfer terms which determine the energetic relations between the mean and eddies over the averaging time. An energy diagram, as shown in Fig. 8, can be used to summarize results and allows some of the general ridge-related characteristics of the global physics to be revealed.

The preferential direction for energy throughput begins with the input by the wind and ends with dissipation of eddy kinetic energy by bottom friction:

$$\text{Wind} \rightarrow \overline{\text{KE}_1} \rightarrow \text{KE}'_1 \rightarrow \text{KE}'_3 \rightarrow \text{Bottom friction.}$$

This was originally found by Holland (1978), who thought it a plausible pathway for the real ocean. Most of the energy coming from the wind is transferred into eddies through a mechanism of barotropic instability in the upper jet. The work done by the eddy pressure forces acting at the interface transfers a part of this energy downward to the lower layer, where it is dissipated by bottom friction. The topography does not fundamentally modify this situation.

Note in Fig. 8 that, while the eddies globally gain energy from the mean kinetic energy through work done by the Reynolds stresses (barotropic instability), the mean flow regains part of this back by a "baroclinic stability" process, i.e., the eddy heat fluxes are such as to transfer energy from the eddy to the mean potential energy of the system. In this global sense the flow is baroclinically stable, although further analysis shows active local regimes of baroclinic instability.

Comparing the two cases, diagram 8 shows that topography seems to have a slight global stabilizing effect on the flows: mean kinetic energy in both layers is increased, eddy kinetic energy is decreased and the corresponding fluxes are generally smaller when topography is present. This effect should mainly concern the barotropic instability which occurs in the strongly shearing jets. In general, the eddy intensity relative to that of the mean flow is far greater than unity in the lower layer. In experiment 1 the global ratio of eddy-to-mean kinetic energy $\text{KE}'_3/\overline{\text{KE}_3}$ is as high as 10.5. It goes down to 7.5 in experiment 2. In the upper layer the eddy-to-mean ratio is of order 2.1 in experiment 1 and goes down to 1.9 in the topographic case. Given the accuracy of the statistics, the other small modifications of the energy fluxes terms are probably not significant.

4. Discussion

Little is known about the combined effect of topography (at any scale) and mesoscale eddies in generating mean flows. However, some tendencies come out from investigations carried out in the context of turbulence studies. Insofar as homogeneous turbulence is con-

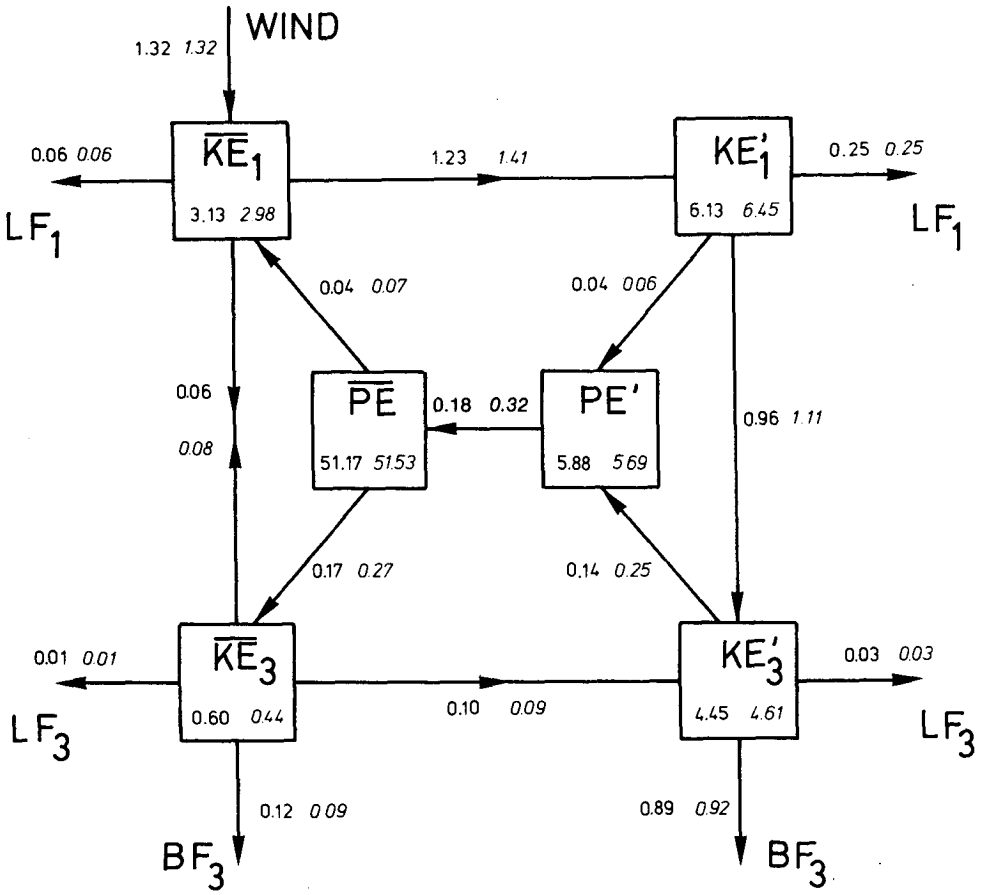

FIG. 8. The global energy diagram in the statistically steady state from experiments 1 (italic) and 2. Units are 10^6 erg cm^{-2} for energies and erg cm^{-2} s^{-1} for energy fluxes.

cerned, Bretherton and Haidvogel (1976) have shown flow to be highly correlated with topography at larger scales. The enstrophy cascade associated with turbulent eddies implies that the flow will tend to approach a state of minimum enstrophy for a given kinetic energy. For flow above a random topography they have shown

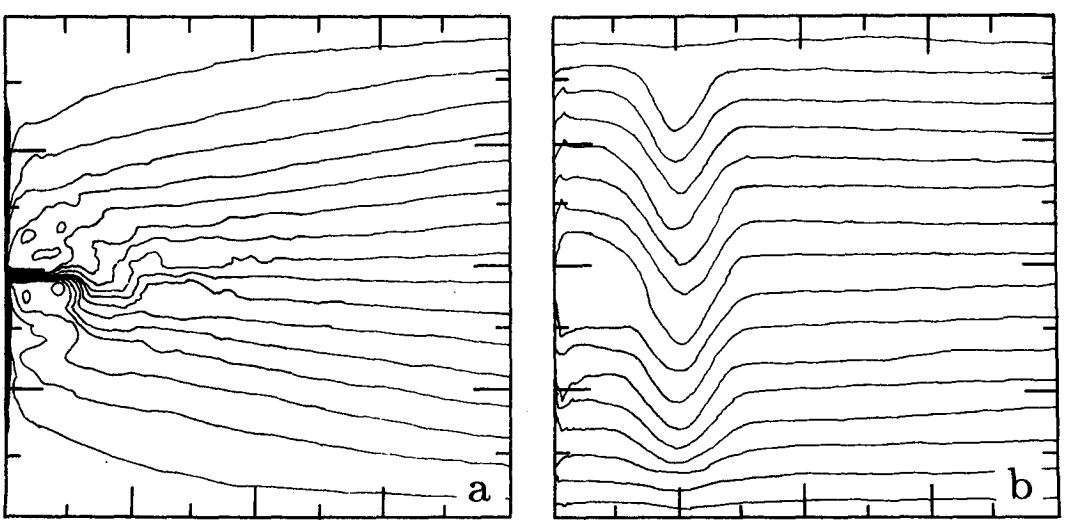

FIG. 9. The mean potential vorticity field in experiment 2. (a) Q_1 and (b) Q_3. (CI = 5×10^{-6} s^{-1}).

that this state features steady streamlines, following the topographic contours on the larger scales but with the finer details smoothed out. The global circulation is then anticyclonic around shallower regions and cyclonic around deeper regions. For flow above a large-scale topography superimposed on a β-effect, depending on the slope, a large-scale flow develops with a new "westward" direction defined to the left of the upslope. This pseudo-westward direction can thus generate fast baroclinic waves. Holloway (1978) and Herring (1977), like Bretherton and Haidvogel (1976), also discuss this emergence of a steady, topographically trapped circulation consisting of anticyclonic circulation around hills. Calculations based on certain simplifying assumptions can be undertaken to estimate how large the mean eddy-driven circulation might be (cf. Rhines and Holland, 1978; Rhines, 1979).

The preceding approaches could be invoked to partially explain the behavior of the deep mean flow occurring over the topography in our experiment 2. In the deep layer, near the topographic feature, the eddy intensity $KE_3'/\overline{KE_3}$ is far greater than unity. Thus, it is relevant to assume the dynamics in this area as being those of a fully eddying situation. The energy input to the eddy field comes mainly from the layer above, through the eddy pressure forces acting at the interface, and the dynamics involved are those of forced turbulence in the presence of large-scale topography. Thus, the average stress exerted by eddies on the Eulerian mean flow has a pseudo-westward component which can strongly modify the general current because advective effects are locally small. In the topographic experiment, two additional mean circulations are induced: a northward circulation over the western flank of the ridge and a southward one over the eastern flank. Assuming spatial homogeneity of the forcing (clearly unreasonable!) the components of the induced velocity might be estimated from the Lagrangian diffusivity. A rough calculation suggests some 5 cm s^{-1} meridional velocity on the western flank of the ridge and some 1 cm s^{-1} on the eastern flank. These estimates are quite consistent with our numerical results.

An interesting supplementary numerical experiment of the kind carried out by Haidvogel and Rhines (1983) would be very useful here. If one were to isolate the deep ocean and treat it as a single layer with transient forcing from above; one could study the secondary induced mean flow and its relationship to the bottom topography. The set up of this flow would be interesting to watch as the pumping action of the eddies sends weak long Rossby waves westward. If the pumping action were over the ridge in the topographic experiment, then new pathways for the spread of energy would be available to complicate those seen in Haidvogel and Rhines' Fig. 2.

However it should be noted that, comparing the above experiment with that analyzed by Holland and Rhines (1980) and the present experiment, there are great differences. This comes from the fact that in the two layer experiment there can be a time averaged form drag on the lower layer, in contrast to the above plunger experiments. A detailed analysis of the Holland and Rhines kind is needed to adequately sort this out, including maps of the vorticity flux vectors and the interesting distortions introduced in the bottom layer by the bathymetry. The conditions for downgradient Q transport by the eddies are well satisfied and this downgradient flux drives the mean abyssal circulation. Topography will distort these somewhat but a clear understanding could be had with such information. This kind of analysis has not been done here but will be left to future work.

Although turbulence studies bring some light to the deep flow behavior, further elucidation is needed for the upper layer and the vertical structure of the flow. In the surface layer, the main signature of the topography is the southward deviation of the jet axis and a tendency for the surface jet to be steered along the f/H contours (or more specifically their QG counterparts). This may be seen as the strongest feature of the topographic influence in terms of the (mean) general circulation. Although the same kind of tendency tends to emerge from the deepest mean flow, baroclinic effects are very important. The surface mean flow is very similar to the interface topography. In particular, the ridge endows this interface with a trough shape, and the upper layer flow follows the interface contours as if they were those of a large scale topographical feature. We observe clearly the maintenance of a baroclinic mean structure against the effects of two-dimensional turbulence towards a more barotropic vertical structure. This has mainly to be due with the topography although horizontal inhomogeneity may also be locally a possible candidate.

As mentioned above, the key to understanding the upper layer flow is a detailed analysis of the equations for the mean vorticities (Holland and Rhines 1980):

$$J\left(\overline{\psi_1}, \overline{\Delta\psi_1} + f + \frac{f_0}{H_1}\overline{h_2}\right) + \overline{J\left(\psi_1', \Delta\psi_1' + \frac{f_0}{H_1}h_2'\right)} = \frac{1}{H_1}\,\mathrm{curl}_z\tau - A\nabla^6\overline{\psi}_1$$

$$J\left(\overline{\psi_3}, \overline{\Delta\psi_3} + f - \frac{f_0}{H_3}\overline{h_2} + \frac{f_0}{H_3}h_0\right) + \overline{J\left(\psi_3', \Delta\psi_3' - \frac{f_0}{H_3}h_2'\right)} = -\epsilon\Delta\overline{\psi}_3 - A\nabla^6\overline{\psi_3}$$

(time-average is denoted with an overbar, fluctuating part with a prime). The various possible balances of all these terms would show us where the eddy terms are important, where the mean interface distortion plays a role as a kind of topographic term acting upon the upper layer. Similarly in the lower layer one could compute the "Sverdrup flow" following the characteristics defined by Q_3, including both bottom bathymetry and interface height in order to determine the impor-

tant forcing terms [$J(\psi'_3, h'_2)$?] that drive the flow across these contours.

Examining more precisely all of these questions will require further analysis of the local vorticity budgets. This is under investigation in a continuing work which also involves a better vertical resolution. But Fig. 10, which is borrowed from that as yet unfinished study, shows the same basic behavior for the surface layer jet with a three-layer model even though the deep mean flow is quasi-motionless over the topographic area.

As far as the patterns of the eddy fields are concerned, the ridge was not observed to have strong remote effects, either on the jet area, or on the geography of the most active eddies. The most striking effect was a modification in the energy radiation from the sources of instabilities. This is concerned therefore with the lowest eddy energy levels for which a significant part of the energy radiation is carried by waves. Thus the interpretation will need to involve basin–wave dynamics in the presence of a large scale topography. The jet acts like a source for the wave radiation within the whole basin. The main effect of the ridge will be the one of the eastward upslope against wave-propagation in combination with β-effect. This problem has been profitably tackled by Suginohara (1981) within the framework of linear theory. He has pointed out the possible free-wave detuning between the two layers in an open ocean because of a large scale topography.

Our simulations come from a very highly idealized model. The degree of generality and scope of applicability to the real ocean are certainly limited. But it seems to be a useful experiment for giving a first step of understanding of the role of the large-scale topography in the oceanic general circulation, and we can expect some of the important ingredients to be present. Notwithstanding the simplicity of the model assumptions, the highly nonlinear dynamical response is fairly complex to be easily and satisfactorily interpreted. Further work is needed and will consider a less crude representation of the vertical stratification as well as carry out a much more extensive range of diagnostic analyses in order to truly understand how the intense surface jet so strongly feels the topographic ridge below.

5. Conclusion

In an attempt to investigate the effect of a midocean ridge on the general circulation and its variability, two numerical simulations, with and without topography, of a two-layer, quasigeostrophic, eddy-resolving model were carried out. Statistical analysis of long term sequences of the quasi-steady state were performed and showed the main effects of the topography to be as follows.

In terms of the general circulation:

- the intense jet stream activity is a little more confined west of the ridge with a tendency for southward turning.

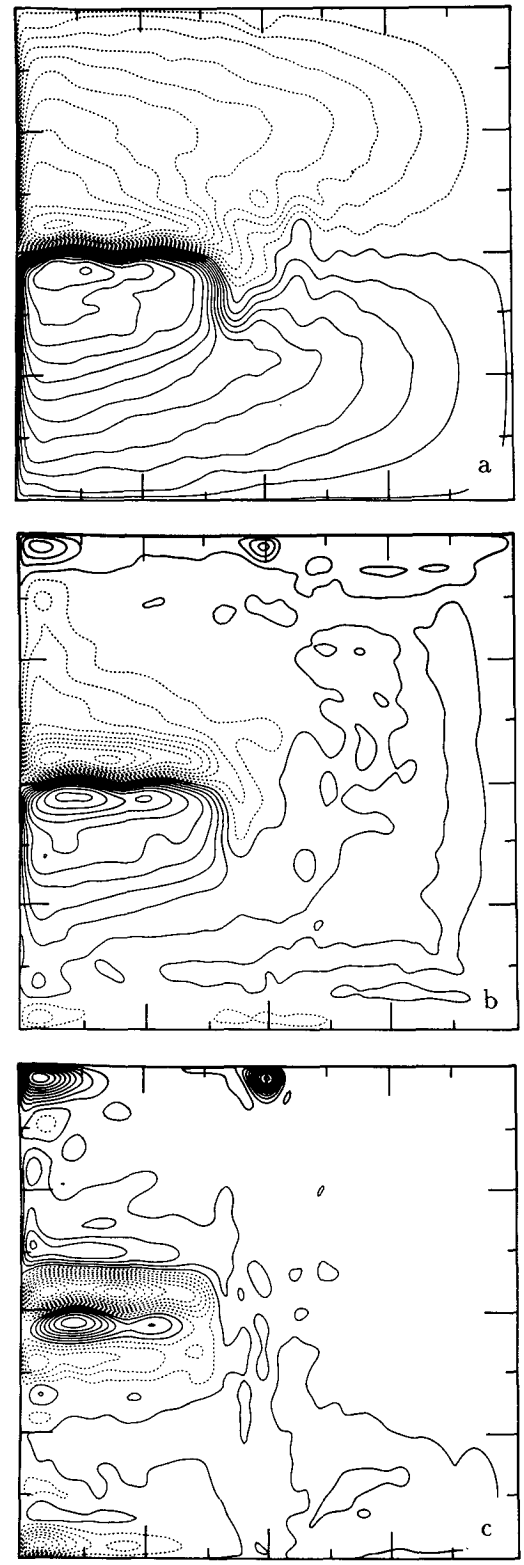

FIG. 10. The mean field in a topographic three-layer experiment from Holland/Colin de Verdière (personal communication, 1986). The numerical parameters are identical except for the followings: $A_4 = 8 \times 10^{10}$ m^4 s^{-1}, $\epsilon = 4 \times 10^{-8}$ s^{-1}, $g'_{12} = 0.0357$ m s^{-2}, $g'_{23} = 0.0162$ m s^{-2}. The topography is given by $h_{max} = 1000$ m, $a = 150$ km, $x_r = 2000$ km. Its zonal shape is also gaussian but no smoothing is provided on north and south boundaries.

- a baroclinic circulation is generated over the topography, anticyclonic in the deep ocean, cyclonic at the surface.
- to a limited extent the ridge acts as a new western boundary for the eastern basin.

There is a spatial redistribution of the horizontal and vertical eddy kinetic energy:

- the ridge has steering and filtering effects on the propagation field of kinetic energy and does not act purely as a barrier.
- these effects are mainly baroclinic in the sense that they are proceeding differently in the two-layers.

Acknowledgments. This work has been supported by the CNRS and the IFREMER through the Programme National d'Etude de la Dynamique des Climats. The calculations have been made with the numerical facilities of the Centre de Calcul Vectoriel pour la Recherche in Palaiseau. W. Holland was supported by the National Science Foundation.

REFERENCES

Bretherton, F. P., and D. B. Haidvogel, 1976: Two-dimensional turbulence above topography. *J. Fluid. Mech.*, **78**, 129–154.

Dantzler, H. L., 1977: Potential energy maxima in the tropical and subtropical North Atlantic. *J. Phys. Oceanogr.*, **7**, 512–519.

Flierl, G., 1978: Models of vertical structure and the calibration of two-layer models. *Dyn. Atmos. Oceans*, **2**, 341–381.

Haidvogel, D. B., and W. H. Holland, 1978: The stability of ocean currents in eddy-resolving general circulation models. *J. Phys. Oceanogr.*, **8**, 393–413.

——, and P. B. Rhines, 1983: Waves and circulation driven by oscillatory winds in an idealized ocean basin. *Geophys. Astrophys. Fluid Dyn.*, **25**, 1–63.

Harrison, D. E., and A. R. Robinson, 1978: Energy analysis of open regions of turbulent mean eddy energetics of a numerical ocean eddy experiment. *Dyn. Atmos. Oceans*, **9**, 919–929.

——, and ——, 1979: Boundary-forced planetary waves: a simple model mid-ocean response to strong current variability. *J. Phys. Oceanogr.*, **2**, 185–211.

——, and W. R. Holland, 1981: Regional eddy vorticity transport and the equilibrium vorticity budgets of a numerical model ocean circulation. *J. Phys. Oceanogr.*, **11**, 1731–1750.

Herring, J. R., 1977: On the statistical theory of two-dimensional topographic turbulence. *J. Atmos. Sci.*, **34**, 1731–1750.

Holland, W. H., and L. B. Lin, 1975a: On the origin of mesoscale eddies and their contribution to the general circulation of the ocean. I. A preliminary numerical experiment. *J. Phys. Oceanogr.*, **5**, 642–756.

——, and ——, 1975b: On the origin of mesoscale eddies and their contribution to the general circulation of the ocean. II. A parameter study. *J. Phys. Oceanogr.*, **5**, 658–669.

Holland, W. R., 1978: The role of mesoscale eddies in the general circulation of the ocean: numerical experiments using a wind-driven quasigeostrophic model. *J. Phys. Oceanogr.*, **8**, 363–392.

——, and P. B. Rhines, 1980: An example of eddy-induced ocean circulation. *J. Phys. Oceanogr.*, **10**, 1010–1031.

——, and W. J. Schmitz, 1985: Zonal penetration scale of model midlatitude jets. *J. Phys. Oceanogr.*, **15**, 1859–1875.

Holloway, G., 1978: A spectral theory of non-linear barotropic motion above irregular topography. *J. Phys. Oceanogr.*, **8**, 414–417.

Rhines, P. B., 1979: Geostrophic turbulence. *Ann. Rev. Fluid Mech.*, **11**, 401–441.

——, and W. R. Holland, 1979: A theoretical discussion of eddy-driven mean flows. *Dyn. Atmos. Oceans*, **3**, 289–325.

Richardson, P. L., 1983: Eddy kinetic energy in the North Atlantic from surface drifters. *J. Geophys. Res.*, **88**, 4355–4367.

Robinson, A. R., E. D. Harrison, Y. Mintz and A. J. Semtner, 1977: Eddies and the general circulation of an idealized gyre: a wind and thermally driven primitive equation numerical experiment. *J. Phys. Oceanogr.*, **7**, 182–207.

Schmitz, W. J., and W. H. Holland, 1982: Numerical eddy resolving general circulation experiments: preliminary comparison with observations. *J. Mar. Res.*, **40**(1), 15–117.

Semtner, A. J., and Y. Mintz, 1977: Numerical simulation of the Gulf Stream and mid-ocean eddies. *J. Phys. Oceanogr.*, **7**, 208–230.

——, and W. H. Holland, 1978: Intercomparison of quasigeostrophic simulation of western North Atlantic circulation with primitive equation results. *J. Phys. Oceanogr.*, **8**, 735–754.

Suginohara, N., 1981: Quasi-geostrophic waves in a stratified ocean with bottom topography. *J. Phys. Oceanogr.*, **11**, 107–115.

Worthington, L. V., 1976: On the North Atlantic circulation. *The Johns Hopkins Oceanographic Studies*, No. 6. The John Hopkins University Press, 110 pp.